

Loop–Loop Interactions Regulate KaiA-Stimulated KaiC Phosphorylation in the Cyanobacterial KaiABC Circadian Clock

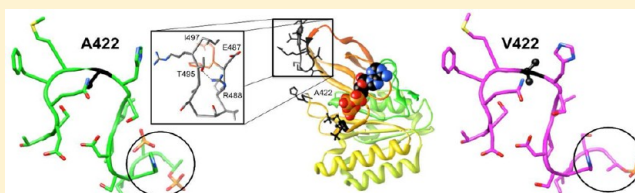
Martin Egli,^{*,†,‡} Rekha Pattanayek,[†] Jonathan H. Sheehan,^{†,‡} Yao Xu,[§] Tetsuya Mori,[§] Jarrod A. Smith,^{‡,‡} and Carl H. Johnson[§]

[†]Department of Biochemistry, Vanderbilt University, School of Medicine, Nashville, Tennessee 37232, United States

[‡]Center for Structural Biology, Vanderbilt University, Nashville, Tennessee 37235, United States

[§]Department of Biological Sciences, College of Arts and Science, Vanderbilt University, Nashville, Tennessee 37235, United States

ABSTRACT: The *Synechococcus elongatus* KaiA, KaiB, and KaiC proteins in the presence of ATP generate a post-translational oscillator that runs in a temperature-compensated manner with a period of 24 h. KaiA dimer stimulates phosphorylation of KaiC hexamer at two sites per subunit, T432 and S431, and KaiB dimers antagonize KaiA action and induce KaiC subunit exchange. Neither the mechanism of KaiA-stimulated KaiC phosphorylation nor that of KaiB-mediated KaiC dephosphorylation is understood in detail at present. We demonstrate here that the A422V KaiC mutant sheds light on the former mechanism. It was previously reported that A422V is less sensitive to dark pulse-induced phase resetting and has a reduced amplitude of the KaiC phosphorylation rhythm in vivo. A422 maps to a loop (422-loop) that continues toward the phosphorylation sites. By pulling on the C-terminal peptide of KaiC (A-loop), KaiA removes restraints from the adjacent 422-loop whose increased flexibility indirectly promotes kinase activity. We found in the crystal structure that A422V KaiC lacks phosphorylation at S431 and exhibits a subtle, local conformational change relative to wild-type KaiC. Molecular dynamics simulations indicate higher mobility of the 422-loop in the absence of the A-loop and mobility differences in other areas associated with phosphorylation activity between wild-type and mutant KaiCs. The A-loop–422-loop relay that informs KaiC phosphorylation sites of KaiA dimer binding propagates to loops from neighboring KaiC subunits, thus providing support for a concerted allosteric mechanism of phosphorylation.



■ ROLE OF PHOSPHORYLATION IN THE KAIABC CIRCADIAN OSCILLATOR FROM THE CYANOBACTERIUM *SYNECHOCOCCUS ELONGATUS*

Cyanobacteria are the simplest organisms known to possess a circadian clock.^{1,2} In *S. elongatus*, the KaiA, KaiB, and KaiC proteins³ constitute a post-translational oscillator (PTO)⁴ that coupled to a transcription/translation oscillatory feedback loop (TTFL)^{5,6} controls protein expression genomewide in a non-promoter specific fashion.^{7,8} The discovery that the KaiA, KaiB, and KaiC proteins from *S. elongatus* in the presence of ATP generate a temperature-compensated oscillator with a 24 h period in a test tube⁴ has now been replicated with the corresponding proteins from the thermophile *Thermosynechococcus elongatus*.⁹ The three Kai proteins interact with each other in vitro and in vivo to form heteromultimeric complexes (Figure 1).^{10–21} The KaiC homo-hexamers,^{13,22} the central component of the clock, is the result of a gene duplication²³ and possesses ATPase,^{24,25} kinase,^{26,27} and ATP synthase/phosphotransferase (dephosphorylation)^{28,29} activities. KaiA stimulates KaiC phosphorylation,^{30,31} and KaiB antagonizes KaiA action,³² whereby binding of KaiB to KaiC coincides with exchange of subunits among hexamers.³³ The KaiC subunit shuffling process appears to be crucial for maintaining a robust amplitude.¹⁶

Phosphorylation and dephosphorylation of KaiC are limited to the C-terminal KaiCII domain,^{34,35} but both the N-terminal KaiCI ring and KaiCII have ATPase activity.^{25,28} Phosphorylation occurs first at T432 and then at S431, and dephosphorylation proceeds in the same order: TS → pTS → pTpS → TpS → TS.^{36,37} The strict order is most likely the result of kinetic control as T432 lies consistently closer to S431 in structures of KaiC.^{13,38} An increasing number of interactions across the subunit interface as a result of phosphorylation renders unfavorable the reverse reaction, forming the basis for a ratcheting mechanism that drives forward the oscillator.¹⁷ In addition to T432 and S431, phosphorylation was also observed at T426 in mutant KaiCs,³⁸ and the T426A mutant is arrhythmic.³⁴ Although T426 has to be phosphorylatable for the clock to function properly,³⁹ S431 and T426 cannot both carry a phosphate at the same time (the side chain of T426 is H-bonded to pS431),³⁸ and the most likely role of T426 is in the stabilization of pS431 and the latter's dephosphorylation.²⁸

A hybrid structural approach involving X-ray crystallography, negative-stain and cryo EM, small-angle X-ray scattering (SAXS), and nuclear magnetic resonance (NMR) has yielded insight into

Received: November 18, 2012

Revised: January 25, 2013

Published: January 25, 2013

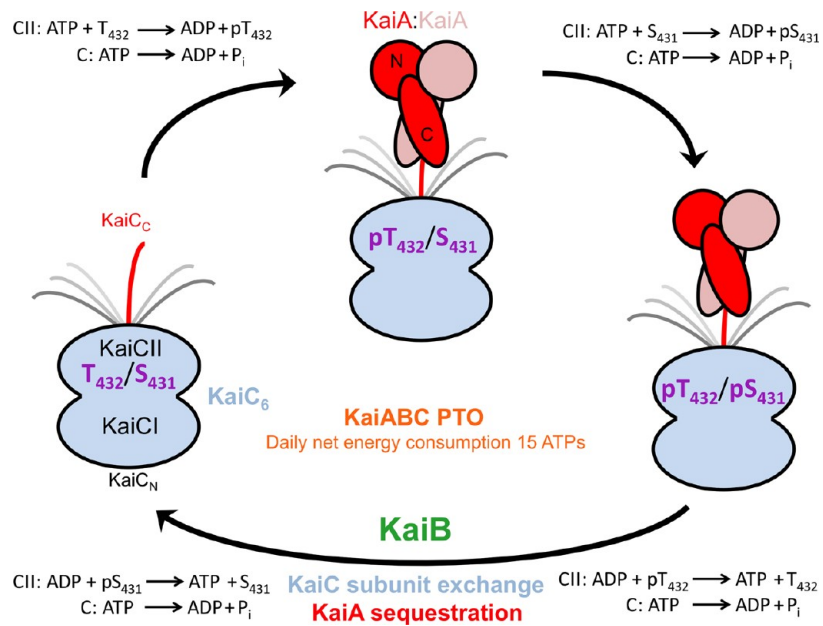


Figure 1. Phosphorylation and dephosphorylation of KaiC during the daily cycle of the KaiABC PTO. KaiC in the hypophosphorylated T432/S431 (TS) state, upon interacting with KaiA dimer via a CII C-terminal peptide, is first phosphorylated at residue T432 (pTS) and then also at residue S431 (pTpS). ATPase activity fuels kinase activity in the CII ring. KaiB dimers associate with the KaiC hexamer in the hyperphosphorylated state. Unlike the C-terminal α -helical bundle domains of KaiA dimer (C-KaiA), KaiB displays no affinity for the C-terminal peptide.¹⁸ Dephosphorylation first of pT432 residues via an ATP synthase mechanism (TpS) and then of pS431 residues leads back to the hypophosphorylated state and is accompanied by KaiC subunit exchange and the appearance of a ternary KaiABC complex in which KaiA is prevented from stimulating KaiC phosphorylation (KaiA sequestration).^{16,21,42}

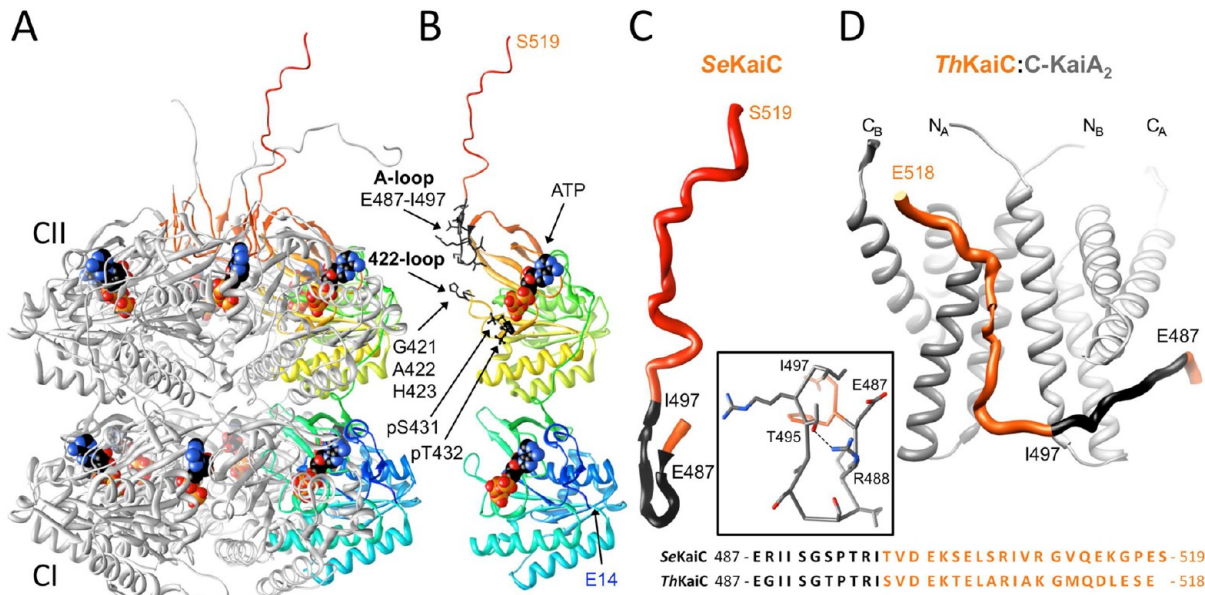


Figure 2. Three-dimensional structures of *S. elongatus* KaiC and the *T. elongatus* KaiA–KaiC peptide complex. (A) Crystal structure of full-length KaiC (Protein Data Bank entry 3DVL).^{13,17} Subunits B–F of the hexamer are colored gray (except for A-loop residues 487–497 that are colored red), and subunit A is shown in rainbow coloring. ATP molecules bound between subunits are shown in space filling mode with carbon atoms colored black. At the N-terminal end of CI (cyan), residues 1–13 are missing in the crystallographic model. C-Terminal peptide tails of CII (red) were traced completely for only subunits A and F.¹⁵ (B) Subunit A depicted separately in the same orientation and coloring as in panel A. N- and C-terminal residues are labeled along with ATPs, the two phosphorylation sites (T432 and S431), and A-loop residues 487–497 and A422-loop residues 421–423 (amino acids in both loops are colored black). (C) Close-up of the conformation of the A-loop (black) and CII-terminal region in the crystal structure. The inset shows the A-loop conformation is stabilized by a hydrogen bond between R488 and T495. (D) NMR solution structure of the complex between the KaiC C-terminal peptide (see panels B and C for coloring) and KaiA dimer (C-terminal domains) from *T. elongatus*.¹⁴ Each KaiA dimer can bind two KaiC peptides, although only one peptide is depicted here. Note the stretched conformation of the former A-loop in the structure of the complex compared to the curled arrangement in the crystal structure (C). An alignment of the sequences of C-terminal regions of KaiCs from *S. elongatus* and *T. elongatus* below panels C and D illustrates that they are highly similar.

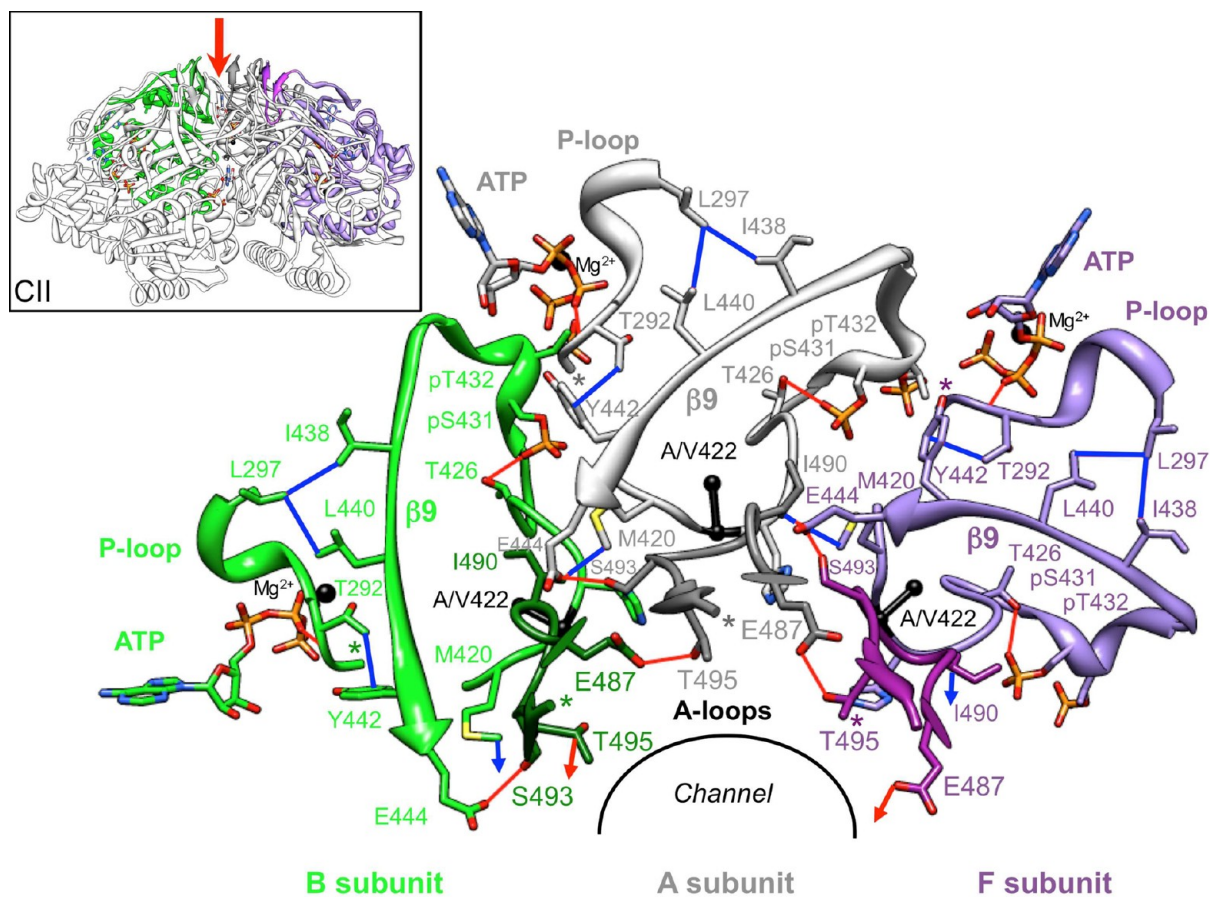


Figure 3. Components of C-terminal KaiCII subunits crucial for relaying A-loop binding by KaiA to the KaiC kinase active site. The view is down the central channel (red arrow in the inset) with N- and C-terminal residues marked with asterisks. A-loops, 422-loops (α and β of A422 are shown as black spheres) and adjacent phosphorylation loop regions, including residues T426, pS431, and pT432, β 9 strands, P-loops, and ATPs (black spheres represent Mg^{2+} ions) are depicted for three neighboring subunits, A (gray), B (green), and F (purple). A-Loops are shown in darker shades; amino acids are labeled, and important hydrogen bonds and hydrophobic contacts linking key structural elements within or across subunits are shown as red and blue lines, respectively. Intrasubunit interactions between the A-loop and the 422-loop are illustrated in more detail in Figures 5 and 6.

the protein–protein interactions over the daily cycle in the KaiABC PTO.^{8,13–21,40} Binding between the C-terminal domains of a KaiA dimer to the C-terminal peptide(s) from the hypophosphorylated form of KaiC hexamer^{13–15} triggers phosphorylation first at T432 and then at S431, ultimately resulting in the hyperphosphorylated form with 12 pT432 and pS431 residues per KaiCII hexamer (Figure 1). KaiB dimers do not compete with KaiA for the same binding site¹⁸ and exhibit the highest affinity for the TpS form.⁴¹ KaiBC complex formation and dephosphorylation coincide with the appearance of another Kai protein complex form with a distinct shape that contains all three proteins.¹⁶ Native polyacrylamide gel electrophoresis (PAGE) experiments using full-length KaiC and a mutant lacking the C-terminal peptide tail indicate that binding of KaiB to KaiC hexamer creates a new binding site for KaiA at the KaiBC interface.⁴² The EM envelope of the ternary complex is consistent with binding of KaiA monomers to the KaiBC particle, and native PAGE confirmed that the N-terminal KaiA pseudoreceiver domain is used for binding.²¹ The KaiBC complex thus sequesters KaiA dimer and prevents it from binding to the C-terminal KaiC peptide(s), an event that is crucial for proper functioning of the clock,^{37,43,44} ultimately bringing about the hypophosphorylated state before the PTO cycle starts anew (Figure 1).

■ UNRAVELING OF THE C-TERMINAL KAIC A-LOOP BY KAIA STIMULATES KAIC KINASE ACTIVITY

The KaiC homo-hexamers take on the shape of a double doughnut with overall dimensions of approximately $100 \text{ \AA} \times 100 \text{ \AA} \times 100 \text{ \AA}$.¹³ A constricted waist in the KaiC barrel marks the boundary between the rings formed by N-terminal KaiCI subunit domains and C-terminal KaiCII subunit domains (Figure 2A). ATP molecules occupy clefts between subunits in both halves such that phosphorylation at T432 and S431 proceeds across the subunit interface (Figures 2A and 3).³⁴ With the exception of the C-terminal region, the CI and CII domains adopt very similar folds (see Figure 2B of ref 13). Residues 245–260 at the C-terminal end of CI act as a linker that adopts an extended conformation between CI and CII. Residues 483–497 near the C-terminus of CII are folded into an S-shaped loop, and the last 22 residues (498–519) protrude from the CII dome and exhibit dynamic conformational behavior (Figure 2). The A-loop consists of residues 487–497, with the hydrogen-bonded R488 and T495 acting as a clamp (Figure 2C). Deletion of the last 30 residues from KaiC ($\Delta 30C$ -KaiC mutant) abolishes circadian rhythmicity, and the R488A mutant displays enhanced damping of rhythmicity.¹⁵

LiWang and co-workers demonstrated using NMR that the C-terminal domains of KaiA dimer bind to the C-terminal region of KaiC comprising residues I490–Q513 (Figure 2D).¹⁴ In the

structure of the C-KaiA–KaiC peptide complex, the A-loop region adopts an extended conformation. Therefore, binding of KaiA unravels the A-loop, thus severing the hydrogen bond between the side chains of R488 and T495 (Figure 2C,D). Interestingly, the KaiC I497 deletion mutant (residues 498–519 deleted) is constitutively hypophosphorylated, and the KaiC E487 deletion mutant (residues 488–519, including the A-loop, deleted) is constitutively hyperphosphorylated.⁴⁵ Moreover, the E487A mutant is arrhythmic and also constitutively hyperphosphorylated. Therefore, the conformation of the KaiC A-loop (extended vs curled) constitutes a circadian phase “switch” that is flipped by KaiA.⁴⁵ Like the E487A mutation, the T495A mutation also confers arrhythmicity,³ and the crystal structure of KaiC provides a rationalization for the more severe consequences of the E487A and T495A mutations compared to those of R488A.¹³ In particular, hydrogen bonds between E487 and T495 residues from adjacent subunits connect A-loops around the entire CII ring (see the illustration with three subunits depicted in Figure 3). Therefore, binding of KaiA to a C-terminal KaiC peptide and concomitant stretching of the A-loop from one subunit can be expected to destabilize the A-loops from neighboring subunits.⁴⁵ Abrogation of this intersubunit hydrogen bonding network as a result of either the E487A or the T495A mutation has drastic consequences in terms of function. In comparison to the T495A mutant that lacks both the intrasubunit hydrogen bond to R488 and the intersubunit hydrogen bond to E487, the R488A mutation results only in the loss of an intrasubunit hydrogen bond and might not alter anything beyond facilitating the transition from the curled to the extended conformation of the A-loop region upon KaiA binding.

Although the conformational changes in the KaiC C-terminal region as a result of docking of KaiA are now hypothetically understood, it is unclear how the unfolding of the A-loop is transmitted to the KaiCII kinase active site beyond a model⁴⁵ that invoked a potential change in ATP orientation triggered by a relay involving the A-loop, the I438–E444 region of strand β 9, and the P-loop (Figure 3). The E444D mutation is thought to disrupt this relay, and the mutant was found to be constitutively hyperphosphorylated.⁴⁵

■ PHENOTYPE OF THE KAIC A422V MUTANT

Some 40000 ethylmethanesulfonate-mutagenized *S. elongatus* strains were screened in terms of their reaction to a 5 h dark pulse. Among many arrhythmic and period-altered mutants, the so-called *pr1* mutant was the only one that retained a normal period but displayed an abnormal response to the dark pulse.⁴⁶ The *pr1* mutation corresponds to an alanine to valine substitution at residue 422 in KaiCII (Figure 2B). KaiC acts as the main repressor of *kaiBC* expression such that overexpression of KaiC represses the activity of its own promoter and temporal overexpression triggers a shift in the phase of the circadian rhythm in a phase-dependent manner. Both functions were affected in the *pr1* mutant. In addition to the inability to shift phase following a dark pulse at any time of the day, the phenotype of the A422V mutant includes (i) the abolished rhythm of KaiC accumulation, (ii) the reduced amplitude of the KaiC phosphorylation rhythm, and (iii) the reduced phase shift compared to that of wild-type *S. elongatus* when KaiC and *pr1*-KaiC were co-expressed in wild-type cells.⁴⁶ A rationale for the drastic changes in clock function as a result of a conservative Ala → Val substitution is currently missing. The A422 residue is in the proximity of the T432 and S431 phosphorylation sites and also maps to one of the so-called KaiA-binding domains,¹¹ i.e.,

the dome-shaped KaiCII surface and residues located beneath it¹³ along with C-terminal A-loops and tentacles (Figure 2).¹⁴ However, a mechanism linking residue 422 to KaiA binding and stimulation of phosphorylation has not yet been proposed.

We hypothesized that the effects displayed by the KaiC A422V mutant on key properties of the cyanobacterial clock, such as the ability to phase shift, the amplitude of KaiC phosphorylation, and rhythmic accumulation of KaiC, should provide key insights into the interaction between KaiA and KaiC and the mechanism of KaiA-stimulated KaiC phosphorylation. Therefore, we undertook a thorough investigation of the structure, stability, and dynamic behavior of the A422V KaiC mutant protein.

■ EXPERIMENTAL PROCEDURES

Protein Expression and Purification. Site-directed mutagenesis of *S. elongatus* KaiC was performed by a modified method of Papworth and co-workers.⁴⁷ The His₆-tagged (C-terminus) KaiC A422V mutant protein was expressed in *Escherichia coli* (BL21 cell line, Novagen/EMD Biochemicals) following earlier protocols for wild-type KaiC.^{13,22} The protein was first purified by metal affinity chromatography (TALON IMAC resin, Takara Bio Clontech) and then by gel filtration chromatography (Sephacryl S-300 HR resin, GE Healthcare). The purity of the protein was assessed by SDS–PAGE and its identity established by trypsin digestion and subsequent analysis by matrix-assisted laser desorption ionization time-of-flight mass spectrometry.

Crystal Structure of the *S. elongatus* KaiC A422V Mutant. The His₆-tagged KaiC A422V mutant protein was crystallized as previously described for wild-type KaiC.¹³ Crystals were flash-frozen and X-ray diffraction data collected on beamline 21-ID-F of the LS-CAT at the Advanced Photon Source (Argonne National Laboratory, Argonne, IL) and processed with HKL2000.⁴⁸ Selected crystal data and data collection parameters are listed in Table 1. The structure was determined by molecular replacement with CNS⁴⁹ and using the native KaiC coordinates [Protein Data Bank (PDB) entry 3DVL]^{15,17} without solvent molecules as the search model. Model building was performed with Coot,⁵⁰ and refinement was conducted with Phenix⁵¹ using all data to 3.3 Å resolution. Final refinement parameters are listed in Table 1.

Crystallographic Data Deposition. Final coordinates and structure factors for the crystallographic model of the *S. elongatus* KaiC A422V mutant protein have been deposited in the Protein Data Bank as entry 4IJM.

CD Melting Experiments. Melting experiments with wild-type (wt) and A422V mutant KaiC were conducted in a quartz cuvette with a 1 mm light path on a Jasco J-810 spectropolarimeter equipped with a Peltier temperature controller. The protein concentration was 0.25 mg/mL (4.3 μ M) in a solution containing 20 mM HEPES–NaOH (pH 8), 100 mM NaCl, 5% glycerol, 1 mM ATP, and 2 mM 2-mercaptoethanol. Thermal denaturation was monitored by recording the ellipticity at 222 nm while the sample was heated from 15 to 95 °C at a rate of 1 °C/min.

Molecular Dynamics Simulations. Starting coordinates for the KaiC simulations were taken from the crystal structure of PDB entry 3DVL.¹⁵ Four variations of the protein were generated manually: wild-type sequence versus A422V mutant, combined with making the C-terminal E487 versus I497. The LEaP program in AmberTools 12 was used to parametrize the systems with the current AMBER ff12SB force field⁵² for the protein, the Meagher et al. parameters⁵³ for the 12 ATP molecules, and the SPC/E water model⁵⁴ and compatible ions.

Table 1. Crystal Data and Refinement Statistics for the KaiC A422V Mutant

Data Collection	
space group	$P2_12_12_1$
unit cell constants (Å)	$a = 131.36, b = 134.47, c = 203.91$
X-ray source	APS, LS-CAT, 21-ID-F
detector	MAR300
wavelength (Å)	0.97872
resolution range (Å) (last shell)	30–3.35 (3.41–3.35)
redundancy (last shell)	6.6 (6.7)
R_{merge} (%)	5.6 (50.3)
no. of unique reflections (last shell)	52438 (2564)
completeness (%) (last shell)	100 (100)
$I/\sigma(I)$ (last shell)	31.1 (2.6)
Refinement	
R_{work} (%)	21.7
R_{free} (%)	26.1
no. of reflections used to calculate R_{free} (%)	5.0
overall average B factor (Å ²)	68.5
no. of protein and ATP atoms	23796
no. of ATP molecules	12
no. of solvent molecules, Mg ²⁺ ions, phosphate ions	397, 7, 8
root-mean-square deviation from ideal geometry	
bonds (Å)	0.007
angles (deg)	0.7
Ramachandran plot (%)	
favored region	90.9
outliers	2.4

LEaP was used to add missing hydrogen atoms, 90 Na⁺ ions for charge neutralization, and to solvate the proteins using 66063 (C-terminal E487) or 66273 water molecules (C-terminal I497) in an orthorhombic box, with an 11 Å clearance to the box edges.

Simulations were performed in AMBER's PMEMD on GPU⁵⁵ using periodic boundary conditions, a real-space cutoff of 9 Å, a Langevin thermostat set to 293 K with $\gamma_{\text{ln}} = 3.0 \text{ ps}^{-1}$, a constant pressure of 1.0 bar with τ_{p} set to 3.0, SHAKE and SETTLE algorithms^{56,57} for bonds involving hydrogen, and a time step of 1.5 fs. Before simulation, the systems were minimized in three stages: first by allowing solvent to relax while the protein was held fixed with strong 1000 kcal mol⁻¹ Å⁻² restraints, then by allowing the protein atoms to relax while the solvent was held fixed with weaker 100 kcal mol⁻¹ Å⁻² restraints, and finally by relaxing the entire system without restraints. After minimization, the systems were equilibrated using seven stages of decreasing restraints on the solute atoms from 16 to 0 kcal mol⁻¹ Å⁻², over the course of 450 ps starting under constant-volume conditions. The last stage of equilibration using weak 0.0625 kcal mol⁻¹ Å⁻² restraints was switched to constant-pressure conditions using isotropic position scaling that were continued for 25 ns with no restraints for production dynamics.

RESULTS

Crystal Structure of the KaiC A422V Mutant. To analyze the effects of replacing alanine with valine at position 422 on the local conformation and the phosphorylation state of KaiC, we determined the crystal structure of the KaiC A422V mutant at 3.3 Å resolution. Crystals of the mutant protein were obtained under conditions very similar to those previously used for wt KaiC and other mutants.^{13,21,28,38} Crystal data, X-ray diffraction data, and

refinement statistics are summarized in Table 1, and a representative example of the quality of the final electron density is depicted in Figure 4A. Inspection of the T432 and S431 phosphorylation sites in CII domains from subunits of the A422V mutant reveals that T432 carries a phosphate in all six and that S431 is not phosphorylated (Figure 5A–F). Thus, the A422V mutant displays a level of phosphorylation that amounts to 60% of the level seen in the crystal structure of wt KaiC [10 phosphates with S431 residues in subunits C (Figure 5H) and D not being phosphorylated].^{13,34} Interestingly, eight phosphate ions are visible in the CI half (Figure 4B,C), undoubtedly the result of hydrolysis of ATP by the ATPase there. Previous structures of the KaiC hexamer did not reveal phosphate ions in the lower ring.

At the structural level, the switch from alanine to valine leads to a subtle conformational adjustment at the apex of the 422-loop as the more bulky valine side chain can no longer be accommodated inside the loop (Figure 5). Thus, the isopropyl moiety swings outward and away from the loop such that its orientation is more or less perpendicular to that of loop main chain atoms. This effect is particularly obvious in subunit C (Figure 5C). By comparison, the methyl side chain of alanine is accommodated in the interior of the loop and therefore lies roughly in the best plane defined by loop residue C α atoms. Despite the different orientations of the alanine and valine side chains, the conformation of the 422-loop exhibits only very minor deviations between the wt and mutant KaiC crystal structures (Figure 6A). As the superimposition of the loops from subunits A in the two structures illustrates, the most significant adjustments occur with the backbone and side chains of residue 422.

In addition to the local rotation of the loop backbone that helps push out the valine side chain in all six subunits of the mutant crystal structure, subunit C displays a conformational change for H423 (Figure 5). Unlike in the rest of the A422V KaiC hexamer, the side chain of H423 there is flipped and thus directed away from the A-loop, resulting in a slight swelling of the 422-loop (Figure 6B). Whereas the change in the loop conformation as a consequence of the Ala \rightarrow Val mutation is essentially limited to the immediate vicinity of residue 422 (Figure 6A), the altered orientation of the H423 side chain in subunit C affects the conformation of the peptide chain for residues S420, G421, V422, and H423 (Figure 6B).

The A-Loop and A422-Loop Are in Direct Contact. As illustrated in Figures 2B, 3, 4A, 5, and 6, the A-loop and the 422-loop are paired and line the KaiC central channel at its C-terminal end. Examination of the distances between residues of the two loops, i.e., S420, G421, A/V422, and H423 (422-loop) and I490, S491, and G492 (A-loop), indicates that the two loops are only weakly associated. In the crystal structure of wt KaiC hexamer, distances between the amide nitrogen of G421 and the carbonyl oxygen of S491 in the six subunits range from 3.27 to 3.77 Å (average of 3.52 Å). For atom pairs at the shorter end of this distance range, it is reasonable to postulate the existence of a weak hydrogen bond. Moreover, the terminal methyl group of the M420 side chain (C ϵ) forms a hydrophobic interaction with C α of G492 (distances range from 3.52 to 4.03 Å; average of 3.77 Å). On the other side of the loop, H423 is too far from I490 to engage in a hydrogen bond or a hydrophobic contact.

Upon examination of the loop–loop interaction in the crystal structure of the A422V KaiC mutant, it becomes clear that there are only minor changes in the distances between paired residues relative to those of wt KaiC. Distances between N(G421) and O(S491) range from 3.37 to 4.23 Å (average of 3.76 Å) in the six

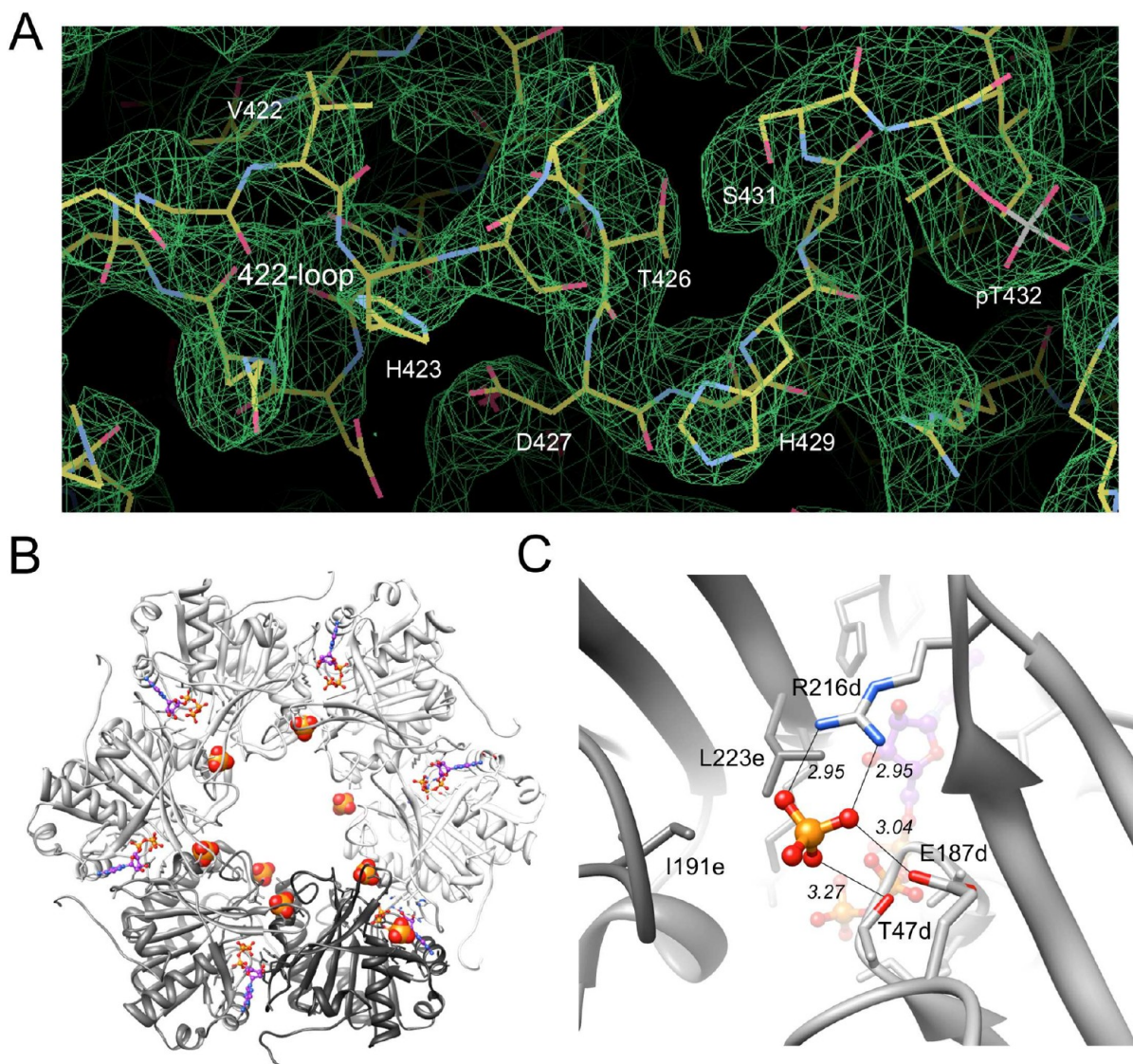


Figure 4. Quality of the KaiC A422V mutant crystal structure and phosphate ion coordination in the CI half. (A) Final $2F_o - F_c$ Fourier sum electron density (1σ threshold) in the region of V422 to pT432 from subunit C. (B) KaiCI ring viewed from the C-terminal side with phosphate ions mostly coordinated near the central channel. ATP molecules bound between subunits of the hexamer (A-subunit, white \rightarrow F-subunit, charcoal) are drawn in ball-and-stick mode. (C) Close-up of the phosphate ion located between subunits D and E. Selected amino acids are depicted as sticks and are labeled, and the coordination geometry is indicated by thin solid lines with distances in angstroms.

subunits, and those between $C\epsilon$ (M420) and Ca (G492) range from 3.49 to 4.37 Å (average of 3.96 Å). The hydrophobic contact involving methionine is therefore not disrupted by the switch from alanine to valine at position 422 and the concomitant local rotation of the loop backbone. However, except for subunit C (Figure 5C), distances between N(G421) and O(S491) (>3.65 Å) are all outside the hydrogen bonding range. The shorter distance there (3.37 Å) may account for a weak stabilization and is related to the flipped orientation of H423 that pushes up the 422-loop, thus moving it closer toward the A-loop (Figure 6B). As this illustration shows, the A-loop maintains an almost identical conformation and orientation despite the closer approach of the 422-loop relative to a subunit with the more common orientation of the histidine side chain in the KaiC A422V mutant structure (Figure 6A). In subunit C, the distance between $C\epsilon$ (M420) and Ca (G492) is 4.17 Å, N(V422) and O(490) are separated by 3.67 Å, and one of the outer methyl

carbons of the V422 side chain ($C\gamma_1$) is 3.72 Å from the side chain of I490 ($C\gamma_2$), consistent with a hydrophobic interaction.

The closer spacing between the side chains of V422 and I490 from the 422- and A-loops, respectively, is clearly related to the altered backbone conformation of the 422-loop in subunit C with the flipped orientation of the H423 side chain. However, the valine side chain jutting away from the loop in the crystal structure of the mutant also aids in the formation of a closer approach between residues 422 and 490. In subunit A, the distance between $C\gamma_1$ (V422) and $C\gamma_2$ (I490) is 4.33 Å, indicative of a hydrophobic interaction. However, in the remaining subunits, this distance is increased and the contacts can no longer be considered to be important for the loop–loop interaction. In the crystal structure of wt KaiC, the orientation of the A422 side chain precludes a hydrophobic contact to side chain atoms of I490 and all distances exceed 7 Å.

The comparison described above between the wt and A422V KaiC crystal structures of the juxtaposition of the A-loop and the

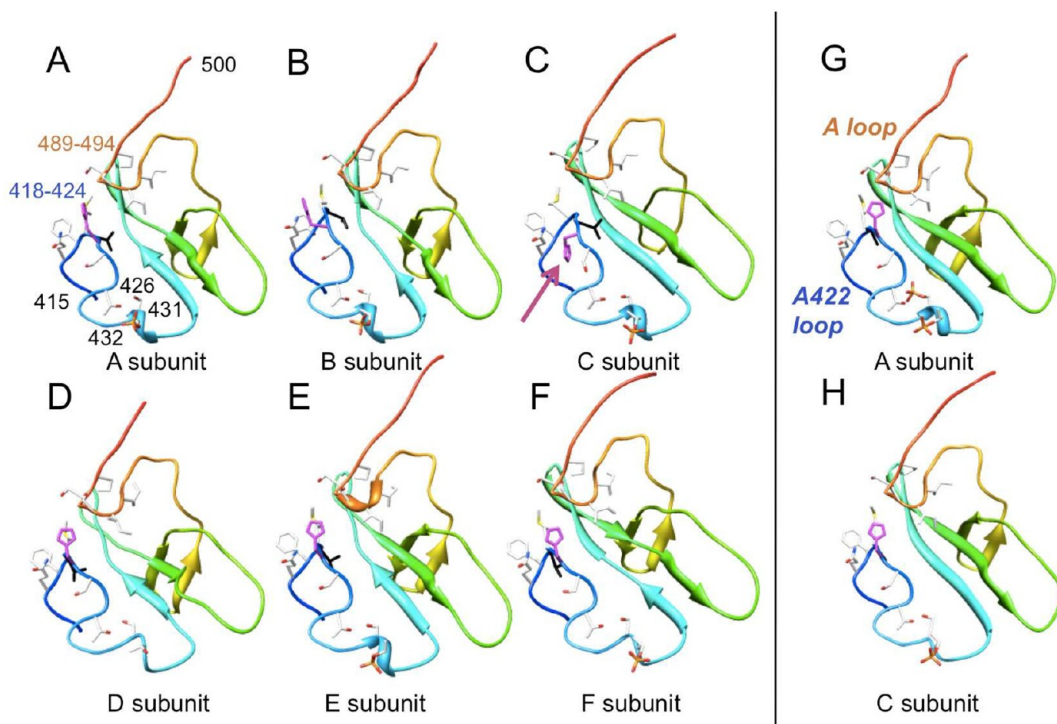


Figure 5. Conformations of the KaiCII C-terminal halves (residues 415–500), including the A-loop and V422-loop in (A–F) all six subunits in the crystal structure of the KaiC A422V mutant. The protein backbone is shown in secondary structure cartoon mode and rainbow coloring. Side chains of selected amino acids are depicted as sticks and labeled, with carbon, oxygen, nitrogen, sulfur, and phosphorus atoms colored gray, red, blue, yellow, and orange, respectively. The V422 side chain is colored black and the H423 side chain magenta. The conformations of the corresponding regions from subunits (G) A and (H) C in the wild-type KaiC crystal structure (PDB entry 3DVL) are shown for comparison (A422 colored black). In subunit C of A422V KaiC, the orientation of H423 is flipped relative to those of all other subunits in both the wt and mutant KaiC crystal structures (arrow in panel C). Note the absence of phosphorylation at S431 in the entire A422V KaiC structure.

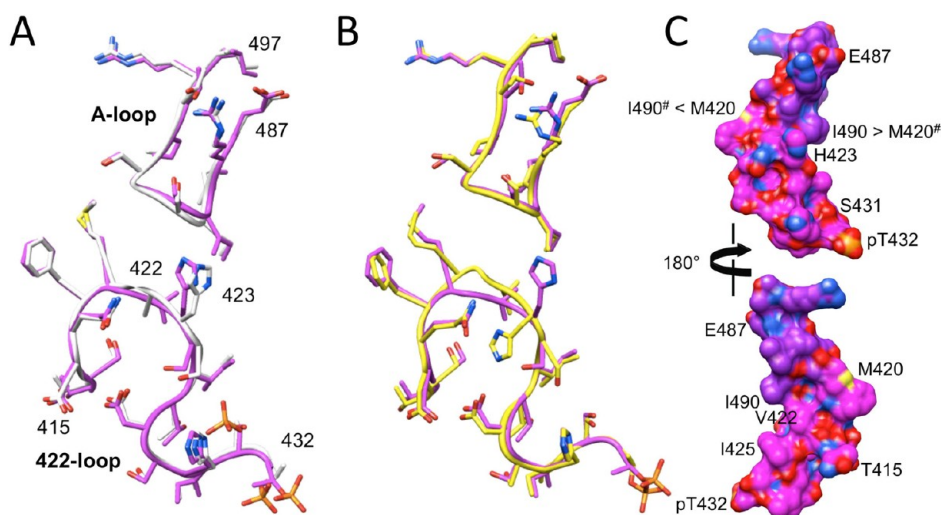


Figure 6. Comparison between the conformations of the A-loop and A/V422-loop regions from selected subunits in the wt KaiC and A422V mutant crystal structures. (A) Superimposition of the loops from subunit A in wt KaiC (gray chain) and A422V KaiC (magenta chain). (B) Superimposition of the loops from subunits A (magenta chain) and C (yellow chain) in A422V KaiC. (C) Surface model of the A-loop–V422-loop van der Waals interaction in KaiCII with pT432 in the foreground (top) and rotated around the vertical by 180° (bottom). Carbon atoms of A-loop and V422-loop residues are colored purple and magenta, respectively, and oxygen, nitrogen, sulfur, and phosphorus atoms are colored red, blue, yellow, and orange, respectively. Selected residues are labeled, and arrows between I490 (A-loop) and M420 (V422-loop) residues indicate hydrophobic contacts between side chains from adjacent subunits (marked by #).

422-loop demonstrates, first, that the two loops are not engaged in a tight interaction and, second, that the Ala → Val mutation does not significantly alter this weak association. Although the spacing of loop backbones and side chains may result in slight

electrostatic and hydrophobic contributions, it may be more appropriate to think of the two loops as essentially engaging in van der Waals interactions. Inspection of a molecular surface model of the A-loop–V422-loop interface illustrates this point

(Figure 6C). Much like an upper lip, the A-loop touches the lower lip, the 422-loop, and neatly seals the gap between them that is apparent in the wire models (Figures 2B, 4A, 5, and 6). However, binding of KaiA to the C-terminal KaiCII peptide opens up the lips by unraveling the A-loop and thus freeing the 422-loop from its constraints.

Thermodynamic Stability of the KaiC A422V Mutant.

To assess a potential effect of the Ala → Val mutation at residue 422 on the stability of KaiC, we conducted CD melting experiments with both the wt and mutant proteins. As shown in Figure 7, the two proteins exhibit virtually identical melting

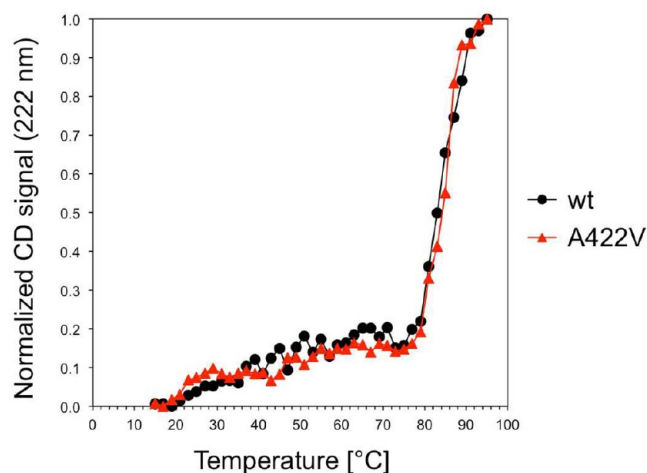


Figure 7. CD melting curves for wild-type and A422V mutant KaiC indicate virtually identical thermodynamic stabilities.

temperatures of ~ 85 °C. Therefore, the manifold changes upon mutation at the functional level cannot be attributed to an altered stability. The similar stabilities of wt KaiC and the A422V KaiC mutant are in line with the outcome of the comparison between the conformations of the two proteins described above. At the structural level, the A422V mutation leads to only minor adjustments at the apex of the 422-loop and its orientation relative to the A-loop in the six subunits. Therefore, changes in the conformation and/or stability of A422V KaiC relative to wt KaiC are unlikely to account for the phenotype of the *prI* mutant⁴⁶ and the reduced level of phosphorylation of the mutant protein in the crystal structure (Figure 5).

Altered Dynamics of the A422-Loop upon Valine Mutation. The observations that the A422V mutation appears not to affect the thermodynamic stability of KaiC and does not change the 422-loop conformation in a substantial way but does attenuate phosphorylation and abrogates phase shifts *in vivo* could indicate that valine at position 422 in the KaiC sequence alters the flexibility of that loop. To examine this hypothesis and determine whether the presence or absence of the adjacent A-loop residues affects the dynamics of the 422-loop, we conducted molecular dynamics (MD) simulations of hexameric, hyperphosphorylated KaiC (residues 14–497, 12 phosphates on T432 and S431) with either A (wt) or V (mutant) at position 422 (A-loop present) and KaiC (residues 14–487) with either A or V at position 422 (A-loop absent, i.e., a mimic of KaiC with KaiA bound). This analysis is based on simulations over 25 ns and focuses on three parameters that represent averages of the six subunits: (i) atomic fluctuations, (ii) root-mean-square deviations (rmsd) relative to the initial conformation, and (iii) distances between $Ca(N390)$ and $Ca(A/V422)$ over the

duration of the simulation (panels A–C of Figure 8, respectively). We chose residue N390 as a reference point in the KaiCII subunit to evaluate the degree of mobility for 422-loop residues as a function of the presence (497) or absence (487) of the A-loop and the identity of the residue at position 422 [A for wt vs V for the mutant (Figure 8)].

Inspection of the graphs depicting the three parameters listed above readily discloses that wt487 and mut487 proteins exhibit higher mobility than their wt497 and mut497 counterparts (Figure 8). Interestingly, in terms of a potential effect of the A422V mutation, the relative fluctuations between wt497 and wt487 hexamers on the one hand and mut497 and mut487 hexamers on the other are quite different. For example, the flexibility of the 422-loop in wt487 increases significantly relative to that of wt497, whereas mut497 and mut487 display similar mobilities. Further along the chain, the region around the phosphorylation sites appears to be somewhat more mobile in the mut497 and mut487 proteins relative to both wt497 and wt487. On the other hand, around E444 (see also Figure 3), wt497 and wt487 exhibit the smallest and largest fluctuations, respectively, whereas mut497 and mut487 behave in a more similar fashion, and the latter's flexibility is reduced relative to that of wt487. Deviating relative fluctuations in these areas could account for altered trends in terms of the phosphorylation of S431 seen in the wt and A422V mutant KaiC forms. Consistent with the higher average mobility of protein residues seen in the simulations of wt487 and mut487 KaiCs relative to the 497 constructs with the A-loop present, ATP molecules in wt487 and mut487 KaiC exhibit elevated mobility relative to those in wt497 and mut497 (Figure 8F). The calculated average fluctuations for 12 ATPs in the four simulated KaiC hexamers are 0.86 Å for wt487, 0.84 Å for mut487, 0.70 Å for wt497, and 0.68 Å for mut497.

Perhaps more surprising than the changes in mobility of residues in the relative proximity of the A- and A/V-422 loops described above is the implication from the MD simulations that the removal of the A-loop appears to alter the dynamic behavior of the hexamer in regions that are relatively distant from residue 422. For example, residues of the KaiCI–CII linker region (residues 245–260) in the wt487 hexamer show higher atomic fluctuations than in the mut487 hexamer (Figure 8A). It is tempting to speculate that these differences might affect the transfer of energy from ATP hydrolysis generated in CI to the CII ring or serve the propagation of conformational changes in CII as a result of KaiA and/or KaiB binding there to CI. A further surprise revealed by the MD simulations concerns the S109–G120 loop regions of subunits at the bottom of the CI ring that exhibit by far the highest mobility in the hexamer [excluding the N- and C-terminal residues (Figure 8A)]. The mobility of these loops appears also to be influenced somewhat by the presence or absence of the A-loops at the opposite end of the KaiC hexamer. To some extent, the higher mobility of residues in this region is related to their surface location. This is consistent with the observation in the crystal structure of KaiC that the loops formed by residues 110–120 display the highest temperature factors apart from the C-terminal tails (not shown). Overall, the MD simulations clearly reveal that the A422V mutation and unraveling of the A-loop affect the relative dynamics of KaiCII residues, whereby the latter event in general leads to a significant mobility increase.

Clearly, it would be desirable to conduct MD simulations for this system on a much longer time scale. However, there is a practical trade-off between the size of the system we simulate and

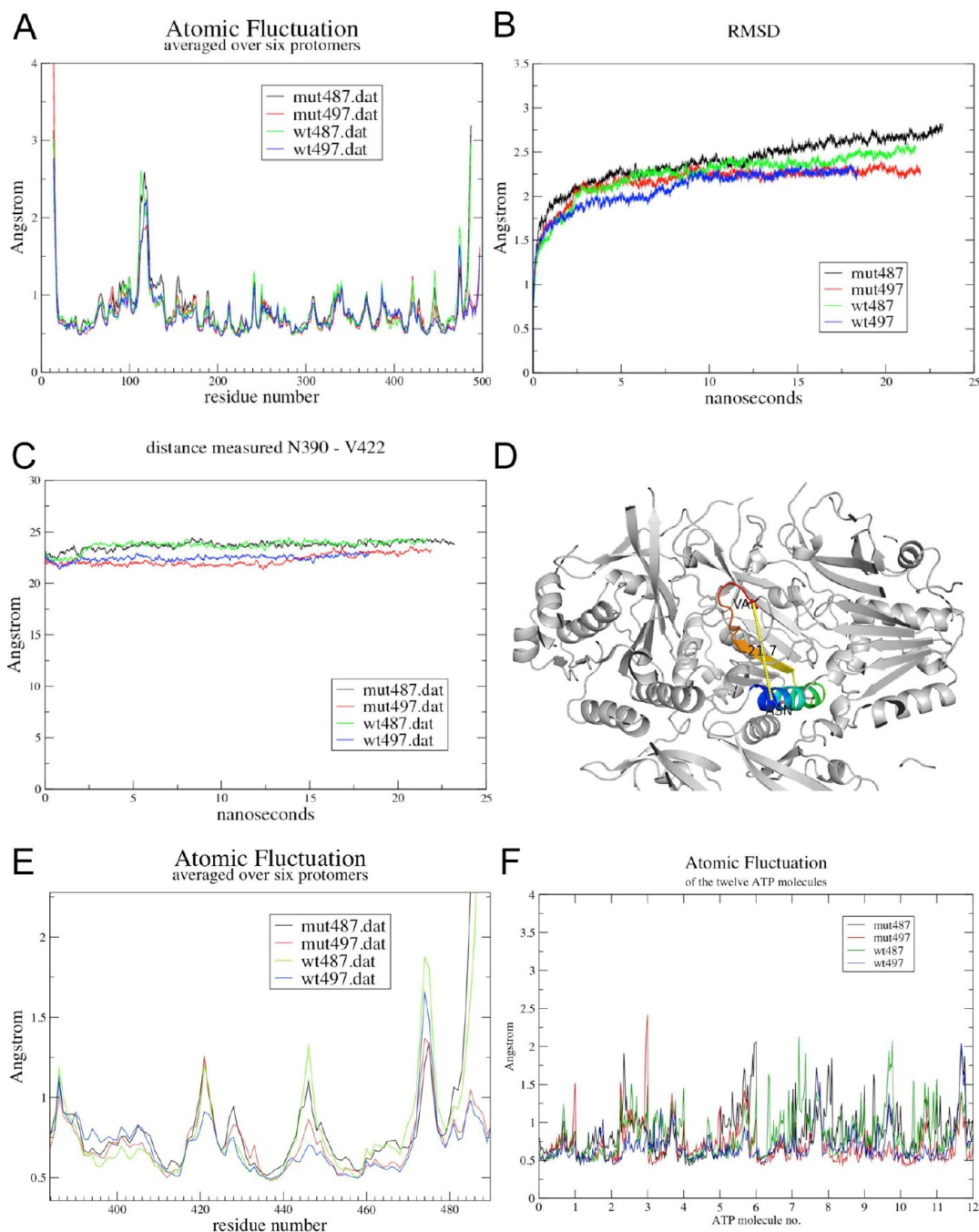


Figure 8. Molecular dynamics (MD) simulations over 25 ns for *S. elongatus* KaiC hexamers with either alanine or valine at position 422 and including A-loop residues (E14–I497; blue and red traces, respectively) or lacking A-loop residues (E14–E487; green and black traces, respectively). Panels depict (A) atomic fluctuations for KaiC residues, (B) root-mean-square deviations (rmsd), (C) variations over the duration of the simulation in panel D [the distance between N390 and A/V422 ($C\alpha$ positions)], (E) close-up of atomic fluctuations for the KaiCII region entailing residues 380–490, and (F) atomic fluctuations for ATP molecules.

the time scale to which we have access. To try to conserve resources, our first attempt comprised a much smaller system: only three CII subunits, which proved to be unstable in the simulation, as did the second attempt, using six CII subunits. Only the full hexameric system remained stable, and only with the use of a gentle seven-stage thermal equilibration protocol described in Experimental Procedures. We have used the short-time scale data that we are able to collect to generate mechanistic interpretations of the molecular system. Also, we have taken advantage of the 6-fold symmetry of the system (which is not enforced during the simulation) to effectively explore conforma-

tional space in an ensemble that is 6 times greater than that of a single subunit. To some extent, this should mitigate the limited time duration of the simulation. At the current stage of our MD simulations (that have been conducted for only the hyperphosphorylated form of KaiC), we cannot satisfactorily answer the question of how phosphorylation (i.e., ST, SpT, pSpT, or pST) affects KaiC dynamics. Clearly, to gain insight into this aspect, we would need to simulate all phosphorylation states and then conduct a detailed comparison among them.

DISCUSSION

KaiA stimulates KaiC phosphorylation and is thus crucial for initiating the rhythmic cycle among the KaiC hypo-, hyper-, and hypophosphorylated states with a period of 24 h that lies at the heart of the cyanobacterial circadian clock. We know that the KaiA dimer binds to KaiC C-terminal peptide(s)^{14,15} and that the conformation of the A-loop region near the C-terminal end of KaiC is altered upon KaiA binding (Figure 2). The observation that a KaiC deletion mutant with the A-loop sequence and the attached C-terminal residues missing (Δ 487-KaiC) is constitutively hyperphosphorylated without KaiA demonstrates the important role played by the A-loop vis-à-vis KaiC phosphorylation.⁴⁵ However, how the A-loop fold observed in the KaiC crystal structure suppresses¹³ and how its unraveling by KaiA activates the KaiCII kinase have remained an enigma. Our concept of the mechanism of KaiA-stimulated KaiC phosphorylation assigns a central role to a loop with residue A422 at its apex (termed 422-loop here) in the activation of KaiC kinase activity at subunit interfaces and phosphorylation of T432 and S431 as a result of KaiA contacting a KaiC C-terminal tail. The A422-loop has so far not been considered in the context of the activation of the KaiC kinase. We provide evidence here based on analyses of the three-dimensional structure, phosphorylation state, and dynamics of the A422V KaiC mutant that together with previous data regarding its phenotype⁴⁶ strongly implicates the 422-loop in the activation of KaiC phosphorylation by KaiA.

Relaying KaiA Binding to the KaiCII Kinase Active Sites.

Because the KaiC phosphorylation–dephosphorylation cycle is so critical for proper functioning of the *S. elongatus* clock, the significant suppression of phosphorylation displayed by the conservative A422V mutation, in addition to its disruption of clock hallmarks such as phase shifting and the rhythm of protein abundance, is particularly striking. The proximity of A422 and the T432 and S431 phosphorylation sites is certainly noteworthy (Figures 2B, 3, and 5), but the fact that the A-loop and the 422-loop are directly associated in the structure of the KaiCII half is particularly interesting with regard to the question of how A-loop unfolding is relayed to the kinase active site. Detailed examination of structural elements in the vicinity of ATP and the two phosphorylation sites reveals a network of interactions that ties together, either directly or indirectly, A-loops, 422-loops (that continue to S431 and T432), β 9 strands, P-loops, and therefore ATP, from individual subunits (Figure 3). A-Loops from adjacent subunits are tethered together by hydrogen bonds between T495 and E487 that are severed upon KaiA binding. A-Loops also engage in interactions with A422-loops from their own (G492–M420) and an adjacent subunit (i.e., I490–M420) and with β 9 strands from the same subunit (S493–E444). From this branch point (A422-loop \leftarrow A-loop \rightarrow β 9), the absence or presence of the A-loop is then relayed both to the phosphorylation region (T432, S431, and T426), via the differential flexibility of the A422-loop, and to the P-loop and therefore ATP, via the β 9 strand [i.e., Y442–E292, L440–L297, and I438–L297 (Figure 3)]. Thus, binding of KaiA to the KaiC C-terminal peptide does not just unravel the A-loop but removes a host of constraints that link the structural elements described above in individual subunits and across the entire KaiCII hexamer, ultimately resulting in greater proximity between T432 and S431 hydroxyl groups and the γ -phosphate of ATP and phosphoryl transfer. It is clear that the order of phosphorylation in KaiCII, T432 first and S431 second,^{36,37} is kinetically

controlled and related to the tighter spacing between T432 and γ P relative to S431 throughout the KaiC structure.^{13,34,38}

Not surprisingly, mutations that alter the interactions among substructures of this network lead to severely distorted periods (e.g., G421R and Y442H) of the clock or loss of rhythmicity (e.g., T495A, E487A, and T426A). Both the T495A³ and E487A⁴⁵ KaiC mutations that disrupt hydrogen bond formation between neighboring A-loops show arrhythmic behavior, and the E487A mutation was also found to be constitutively hyperphosphorylated. We have described the consequences of the A422V mutation⁴⁶ for clock function and how it relates to KaiA-stimulated KaiC phosphorylation in detail in this work. In addition, the G421R mutation that can be expected to alter the A-loop–A422-loop interface exhibits a clock period of 44 h.³ Closer to the phosphorylation sites, the T426A mutant has long been known to be arrhythmic.^{34,38,39} The side chain of T426 engages in a direct interaction with the phosphate on S431,^{13,34} and because we envision an important role of the short peptide stretch between A422 and S431/T432 in transmitting the increased flexibility of the A422-loop as a result of the removal of the A-loop by KaiA to the phosphorylation sites, it is not surprising that T426 mutations would be detrimental to clock function. In the context of changed network interactions as a result of binding of KaiA to the A-loop region that affect β 9, P-loop, and ultimately ATP phosphates, it is noteworthy that the Y442H mutation lengthens the clock period to 60 h.³ Overall, the available point mutation data are consistent with a key role of these structural elements in the regulation of phosphorylation.

Concerted Allostery of KaiA Stimulation. “Pulling” by KaiA on the C-terminal tail and the attached A-loop from a single KaiC subunit will affect the subunits to its left and right as well. This is because of the aforementioned network of interactions that links adjacent subunits at the level of the A- and 422-loops. From the first affected subunit, there will be a spiraling cascade of phosphorylations around the KaiCII hexamer on T432 residues that progress to spiraling phosphorylations of S431 residues. This network of intramolecular interactions results in a “domino effect” of phosphorylations jumping from one subunit to the next. Therefore, it seems unnecessary to invoke a model with a KaiA dimer migrating from one KaiC subunit to the next⁵⁸ or two or more KaiA dimers simultaneously binding to multiple KaiC tails. In fact, it was found early on in the study of the cyanobacterial clock that a single KaiA dimer is sufficient to upregulate phosphorylation of a KaiC hexamer to the maximal level.⁵⁹ Consequently, an allosteric mechanism of KaiA-stimulated KaiC autophosphorylation is more appealing.⁶⁰ Concerted allosteric control is not just in line with the hexameric nature of KaiC and the intriguing network of interactions among subunits in the region of KaiA–KaiC interactions (Figure 3) and elsewhere in the KaiC hexamer but is also consistent with the relative concentrations and/or stoichiometries of Kai proteins in the cell³³ and in the *in vitro* reaction.⁴ Thus, the cellular concentrations of the KaiB and KaiC proteins are estimated to be 10–30 μ M, and the concentration of KaiA is estimated to be 0.5–1 μ M. Further support for the concerted allosteric model comes from the KaiA–KaiC binding mode. Although Figure 2D depicts only a single KaiC peptide chain bound between the C-terminal domains from a KaiA dimer, each KaiA dimer can in principle bind two KaiC peptides.¹⁴ The three-dimensional model of the KaiA–KaiC complex based on electron microscopy^{15,20} is not of sufficient resolution to determine whether KaiA is tethered to two KaiC C-terminal peptides in all cases. However, the illustrations in Figure 3 make it clear that

unfolding by KaiA of A-loops from two KaiC subunits that are not direct neighbors in the hexamer will loosen the association among all six subunits.

The mechanism proposed here in regard to the stimulation of KaiC phosphorylation by KaiA is compatible with the ratcheting concept for KaiC phosphorylation,¹⁷ i.e., why time in the in vitro oscillator is unidirectional.⁸ This is because the stimulation mechanism does not affect the order of phosphorylation that is kinetically controlled and the fact that phosphorylation of T432 results in an increased number of interactions between residues across the subunit interface, thus promoting the next step, phosphorylation of S431.

Structural Basis of the A422V Phenotype. Recent research has provided crucial insights into two sources of metabolic input to the circadian oscillator that allow cyanobacteria to sense the daily light–dark cycle. Thus, KaiC phosphorylation is directly affected by the cellular ATP/ADP ratio that itself depends on photophosphorylation.⁶¹ In fact, changes in the ATP/ADP ratio were also demonstrated to reset the phase of KaiC phosphorylation in the in vitro oscillation reaction mixture constituted by KaiA, KaiB, and KaiC in the presence of ATP. A second metabolic signal that influences the phase of the KaiABC PTO is related to the oxidation state of the plastoquinone (PQ) pool.⁶² Oxidized PQ causes KaiA aggregation⁶² and interferes with binding of KaiA to the KaiC C-terminal peptide,⁶³ thus limiting stimulation of phosphorylation of KaiC by KaiA. These two cues, oxidized PQ and ATP/ADP ratio, appear to act in tandem to signal the onset of darkness (when the PQ pool becomes oxidized rapidly) and to measure the duration of darkness (triggering a slow decline of the ATP/ADP ratio that induces a phase shift), respectively.⁶⁴

Both metabolic input signals serving entrainment of the cyanobacterial oscillator therefore affect KaiC phosphorylation. This suggests that the inability of the KaiC A422V mutant to shift phase could be directly related to its distorted phosphorylation [i.e., the low amplitude of the phosphorylation cycle⁴⁶ and the inability to phosphorylate S431 (this paper, Figure 4A)]. We have shown here that the A422V mutant's defective phosphorylation may be the result of an altered mobility of its 422-loops and adjacent regions relative to wt KaiC, precipitated by KaiA binding and concomitant unraveling of A-loops. Relaying by the 422-loop the removal of restraints exerted by A-loops to the phosphorylation sites and P-loops and/or ATP involves numerous hydrophobic contacts [A-loop–422-loop, β 9–P-loop, etc. (Figure 3)]. Unlike other noncovalent interactions, such as hydrogen bonds or van der Waals forces, hydrophobic interactions become weaker as the temperature is lowered.⁶⁵ That hydrophobics play a crucial role in the transmission of binding of KaiA to the KaiC kinase active site may be supported by the observation that KaiC becomes hyperphosphorylated at a low temperature (4 °C) relative to ambient conditions.⁴² It is also possible that the A422V mutation directly affects KaiA–KaiC binding and the ability of KaiA to pull on the KaiC tail and unravel the A-loop.

In summary, an apparently minor change in a residue from alanine to valine at position 422 in the cyanobacterial master clock protein KaiC gives rise to drastic changes at the functional level that include an inability to reset the phase and distorted phosphorylation. This analysis of the structure, phosphorylation pattern, stability, and dynamics of the KaiC A422V mutant provides a much-improved understanding of the mechanism of KaiA-stimulated KaiC phosphorylation.

AUTHOR INFORMATION

Corresponding Author

*Department of Biochemistry, Vanderbilt University, School of Medicine, 607 Light Hall, Nashville, TN 37232-0146. Telephone: (615) 343-8070. Fax: (615) 322-7122. E-mail: martin.egli@vanderbilt.edu.

Funding

We are grateful to the National Institutes of Health for supporting clock research in our laboratories (Grants R01 GM073845 to M.E. and R01 GM067152 to C.H.J.). Use of the Advanced Photon Source was supported by the U.S. Department of Energy, Office of Science, Office of Basic Energy Sciences, under Contract DE-AC02-06CH11357. Use of LS-CAT Sector 21 was supported by the Michigan Economic Development Corp. and the Michigan Technology Tri-Corridor for the support of this research program (Grant 08SP1000817).

Notes

The authors declare no competing financial interest.

ACKNOWLEDGMENTS

We thank Dr. Spencer Anderson (LS-CAT, Advanced Photon Source, Argonne National Laboratory) for help with X-ray data collection and Prof. Terry Lybrand (Vanderbilt University) for helpful discussions.

REFERENCES

- (1) Johnson, C. H. (2004) Precise circadian clocks in prokaryotic cyanobacteria. *Curr. Issues Mol. Biol.* 6, 103–110.
- (2) Ditty, J. L., Mackey, S. R., and Johnson, C. H., Eds. (2009) *Bacterial Circadian Programs*, Springer Publishers Inc., Heidelberg, Germany.
- (3) Ishiura, M., Kutsuna, S., Aoki, S., Iwasaki, H., Andersson, C. R., Tanabe, A., Golden, S. S., Johnson, C. H., and Kondo, T. (1998) Expression of a gene cluster *kaiABC* as a circadian feedback process in cyanobacteria. *Science* 281, 1519–1523.
- (4) Nakajima, M., Imai, K., Ito, H., Nishiwaki, T., Murayama, Y., Iwasaki, H., Oyama, T., and Kondo, T. (2005) Reconstitution of circadian oscillation of cyanobacterial KaiC phosphorylation in vitro. *Science* 308, 414–415.
- (5) Tomita, J., Nakajima, M., Kondo, T., and Iwasaki, H. (2005) Circadian rhythm of KaiC phosphorylation without transcription-translation feedback. *Science* 307, 251–254.
- (6) Qin, X., Byrne, M., Yu, X., Mori, T., and Johnson, C. H. (2010) Coupling of a core post-translational pacemaker to a slave transcription/translation feedback loop in a circadian system. *PLoS Biol.* 8, e1000394.
- (7) Xu, Y., Mori, T., and Johnson, C. H. (2000) Circadian clock-protein expression in cyanobacteria: Rhythms and phase setting. *EMBO J.* 19, 3349–3357.
- (8) Johnson, C. H., Stewart, P. L., and Egli, M. (2011) The cyanobacterial circadian system: From biophysics to bioevolution. *Annu. Rev. Biophys.* 40, 143–167.
- (9) Murakami, R., Mutoh, R., Iwase, R., Furukawa, Y., Imada, K., Onai, K., Morishita, M., Yasui, S., Ishii, K., Valencia Swain, J. O., Uzumaki, T., Namba, K., and Ishiura, M. (2012) The roles of the dimeric and tetrameric structures of the clock protein KaiB in the generation of circadian oscillations in cyanobacteria. *J. Biol. Chem.* 287, 29506–29015.
- (10) Iwasaki, H., Taniguchi, Y., Kondo, T., and Ishiura, M. (1999) Physical interactions among circadian clock proteins, KaiA, KaiB and KaiC, in cyanobacteria. *EMBO J.* 18, 1137–1145.
- (11) Taniguchi, Y., Yamaguchi, A., Hijikata, A., Iwasaki, H., Kamagata, K., Ishiura, M., Go, M., and Kondo, T. (2001) Two KaiA-binding domains of cyanobacterial circadian clock protein KaiC. *FEBS Lett.* 496, 86–90.
- (12) Kageyama, H., Kondo, T., and Iwasaki, H. (2003) Circadian formation of clock protein complexes by KaiA, KaiB, KaiC, and SasA in cyanobacteria. *J. Biol. Chem.* 278, 2388–2395.

- (13) Pattanayek, R., Wang, J., Mori, T., Xu, Y., Johnson, C. H., and Egli, M. (2004) Visualizing a circadian clock protein: Crystal structure of KaiC and functional insights. *Mol. Cell* 15, 375–388.
- (14) Vakonakis, I., and LiWang, A. C. (2004) Structure of the C-terminal domain of the clock protein KaiA in complex with a KaiC-derived peptide: Implications for KaiC regulation. *Proc. Natl. Acad. Sci. U.S.A.* 101, 10925–10930.
- (15) Pattanayek, R., Williams, D. R., Pattanayek, S., Xu, Y., Mori, T., Johnson, C. H., Stewart, P. L., and Egli, M. (2006) Analysis of KaiA-KaiC protein interactions in the cyanobacterial circadian clock using hybrid structural methods. *EMBO J.* 25, 2017–2038.
- (16) Mori, T., Williams, D. R., Byrn, M., Qin, X., Egli, M., Mchaourab, H., Stewart, P. L., and Johnson, C. H. (2007) Elucidating the ticking of an in vitro circadian clockwork. *PLoS Biol.* 5, e93.
- (17) Johnson, C. H., Egli, M., and Stewart, P. L. (2008) Structural insights into a circadian oscillator. *Science* 322, 697–701.
- (18) Pattanayek, R., Williams, D. R., Pattanayek, S., Mori, T., Johnson, C. H., Stewart, P. L., and Egli, M. (2008) Structural model of the circadian clock KaiB-KaiC complex and mechanism for modulation of KaiC phosphorylation. *EMBO J.* 27, 1767–1778.
- (19) Akiyama, S., Nohara, A., Ito, K., and Maéda, Y. (2008) Assembly and disassembly dynamics of the cyanobacterial periodosome. *Mol. Cell* 29, 703–716.
- (20) Egli, M., and Stewart, P. L. (2009) Structural aspects of the cyanobacterial KaiABC circadian clock. In *Bacterial Circadian Programs* (Ditty, J. L., Mackey, S. R., and Johnson, C. H., Eds) pp 121–140, Springer Publishers Inc., Heidelberg, Germany.
- (21) Pattanayek, R., Williams, D. R., Rossi, G., Weigand, S., Mori, T., Johnson, C. H., Stewart, P. L., and Egli, M. (2011) Combined SAXS/EM based models of the *S. elongatus* posttranslational oscillator and its interactions with the output His-kinase SasA. *PLoS One* 6, e23697.
- (22) Mori, T., Saveliev, S. V., Xu, Y., Stafford, W. F., Cox, M. M., Inman, R. B., and Johnson, C. H. (2002) Circadian clock protein KaiC forms ATP-dependent hexameric rings and binds DNA. *Proc. Natl. Acad. Sci. U.S.A.* 99, 17203–17208.
- (23) Leipe, D. D., Aravind, L., Grishin, N. V., and Koonin, E. V. (2000) The bacterial replicative helicase DnaB evolved from a RecA duplication. *Genome Res.* 10, 5–16.
- (24) Terauchi, K., Kitayama, Y., Nishiwaki, T., Miwa, K., Murayama, Y., Oyama, T., and Kondo, T. (2007) The ATPase activity of KaiC determines the basic timing for circadian clock of cyanobacteria. *Proc. Natl. Acad. Sci. U.S.A.* 104, 16377–16381.
- (25) Murakami, R., Miyake, A., Iwase, R., Hayashi, F., Uzunaki, T., and Ishiura, M. (2008) ATPase activity and its temperature compensation of the cyanobacterial clock protein KaiC. *Genes Cells* 13, 387–395.
- (26) Nishiwaki, T., Iwasaki, H., Ishiura, M., and Kondo, T. (2000) Nucleotide binding and autophosphorylation of the clock protein KaiC as a circadian timing process of cyanobacteria. *Proc. Natl. Acad. Sci. U.S.A.* 97, 495–499.
- (27) Iwasaki, H., Nishiwaki, T., Kitayama, Y., Nakajima, M., and Kondo, T. (2002) KaiA-stimulated KaiC phosphorylation in circadian timing loops in cyanobacteria. *Proc. Natl. Acad. Sci. U.S.A.* 99, 15788–15793.
- (28) Egli, M., Mori, T., Pattanayek, R., Xu, Y., Qin, X., and Johnson, C. H. (2012) Dephosphorylation of the core clock protein KaiC in the cyanobacterial KaiABC circadian oscillator proceeds via an ATP synthase mechanism. *Biochemistry* 51, 1547–1558.
- (29) Nishiwaki, T., and Kondo, T. (2012) Circadian autodephosphorylation of cyanobacterial clock protein KaiC occurs via formation of ATP as intermediate. *J. Biol. Chem.* 287, 18030–18035.
- (30) Williams, S. B., Vakonakis, I., Golden, S. S., and LiWang, A. C. (2002) Structure and function from the circadian clock protein KaiA of *Synechococcus elongatus*: A potential clock input mechanism. *Proc. Natl. Acad. Sci. U.S.A.* 99, 15357–15362.
- (31) Xu, Y., Mori, T., and Johnson, C. H. (2003) Cyanobacterial circadian clockwork: Roles of KaiA, KaiB, and the *kaiBC* promoter in regulating KaiC. *EMBO J.* 22, 2117–2126.
- (32) Kitayama, Y., Iwasaki, H., Nishiwaki, T., and Kondo, T. (2003) KaiB functions as an attenuator of KaiC phosphorylation in the cyanobacterial circadian clock system. *EMBO J.* 22, 1–8.
- (33) Kageyama, H., Nishiwaki, T., Nakajima, M., Iwasaki, H., Oyama, T., and Kondo, T. (2006) Cyanobacterial circadian pacemaker: Kai protein complex dynamics in the KaiC phosphorylation cycle in vitro. *Mol. Cell* 23, 161–171.
- (34) Xu, Y., Mori, T., Pattanayek, R., Pattanayek, S., Egli, M., and Johnson, C. H. (2004) Identification of key phosphorylation sites in the circadian clock protein KaiC by crystallographic and mutagenetic analyses. *Proc. Natl. Acad. Sci. U.S.A.* 101, 13933–13938.
- (35) Nishiwaki, T., Satomi, Y., Nakajima, M., Lee, C., Kiyohara, R., Kageyama, H., Kitayama, Y., Temamoto, M., Yamaguchi, A., Hijikata, A., Go, M., Iwasaki, H., Takao, T., and Kondo, T. (2004) Role of KaiC phosphorylation in the circadian clock system of *Synechococcus elongatus* PCC 7942. *Proc. Natl. Acad. Sci. U.S.A.* 101, 13927–13932.
- (36) Nishiwaki, T., Satomi, Y., Kitayama, Y., Terauchi, K., Kiyohara, R., Takao, T., and Kondo, T. (2007) A sequential program of dual phosphorylation of KaiC as a basis for circadian rhythm in cyanobacteria. *EMBO J.* 26, 4029–4037.
- (37) Rust, M. J., Markson, J. S., Lane, W. S., Fisher, D. S., and O'Shea, E. K. (2007) Ordered phosphorylation governs oscillation of a three-protein circadian clock. *Science* 318, 809–812.
- (38) Pattanayek, R., Mori, T., Xu, Y., Pattanayek, S., Johnson, C. H., and Egli, M. (2009) Structures of KaiC circadian clock mutant proteins: A new phosphorylation site at T426 and mechanisms of kinase, ATPase and phosphatase. *PLoS One* 4, e7529.
- (39) Xu, Y., Mori, T., Qin, X., Yan, H., Egli, M., and Johnson, C. H. (2009) Intramolecular regulation of phosphorylation status of the circadian clock protein KaiC. *PLoS One* 4, e7509.
- (40) Chang, Y.-G., Tseng, R., Kuo, N.-W., and LiWang, A. (2012) Rhythmic ring-ring stacking drives the circadian oscillator clockwise. *Proc. Natl. Acad. Sci. U.S.A.* 109, 16847–16851.
- (41) Murayama, Y., Mukaiyama, A., Imai, K., Onoue, Y., Tsunoda, A., Nohara, A., Ishida, T., Maéda, Y., Terauchi, K., Kondo, T., and Akiyama, S. (2011) Tracking and visualizing the circadian ticking of the cyanobacterial clock protein KaiC in solution. *EMBO J.* 30, 68–78.
- (42) Qin, X., Byrne, M., Mori, T., Zou, P., Williams, D. R., Mchaourab, H., and Johnson, C. H. (2010) Intermolecular associations determine the dynamics of the circadian KaiABC oscillator. *Proc. Natl. Acad. Sci. U.S.A.* 107, 14805–14810.
- (43) Brettschneider, C., Rose, R. J., Hertel, S., Axmann, I. M., Heck, A. J. R., and Kollmann, M. (2010) A sequestration feedback determines dynamics and temperature entrainment of the KaiABC circadian clock. *Mol. Syst. Biol.* 6, 389.
- (44) Markson, J. S., and O'Shea, E. K. (2009) The molecular clockwork of a protein-based circadian oscillator. *FEBS Lett.* 583, 3938–3947.
- (45) Kim, Y.-I., Dong, G., Carruthers, C., Golden, S. S., and LiWang, A. (2008) A day/night switch in KaiC, a central oscillator component of the circadian clock of cyanobacteria. *Proc. Natl. Acad. Sci. U.S.A.* 105, 12825–12830.
- (46) Kiyohara, Y. B., Katayama, M., and Kondo, T. (2005) A novel mutation in *kaiC* affects resetting of the cyanobacterial circadian clock. *J. Bacteriol.* 187, 2559–2564.
- (47) Papworth, C., Bauer, J. C., Braman, J., and Wright, D. A. (1996) Site-directed mutagenesis using double-stranded plasmid DNA templates. *Strategies* 9, 3–4.
- (48) Otwinowski, Z., and Minor, W. (1997) Processing of X-ray diffraction data collected in oscillation mode. *Methods Enzymol.* 276, 307–326.
- (49) Brünger, A. T., Adams, P. D., Clore, G. M., DeLano, W. L., Gros, P., Grosse-Kunstleve, R. W., Jiang, J. S., Kuszewski, J., Nilges, M., Pannu, N. S., Read, R. J., Rice, L. M., Simonson, T., and Warren, G. L. (1998) Crystallography & NMR System: A new software suite for macromolecular structure determination. *Acta Crystallogr. D* 54, 905–921.
- (50) Emsley, P., and Cowtan, K. (2004) Coot: Model-building tools for molecular graphics. *Acta Crystallogr. D* 60, 2126–2132.
- (51) Adams, P. D., Afonine, P. V., Bunkoczi, G., Chen, V. B., Davis, I. W., Echols, N., Headd, J. J., Hung, L. W., Kapral, G. J., Grosse-Kunstleve,

R. W., McCoy, A. J., Moriarty, N. W., Oeffner, R., Read, R. J., Richardson, J. S., Terwilliger, T. C., and Zwart, P. H. (2010) PHENIX: A comprehensive Python-based system for macromolecular structure solution. *Acta Crystallogr. D* 66, 213–221.

(52) Case, D. A., Darden, T. A., Cheatham, T. E., III, Simmerling, C. L., Wang, J., Duke, R. E., Luo, R., Walker, R. C., Zhang, W., Merz, K. M., Roberts, B., Hayik, S., Roitberg, A., Seabra, G., Swails, J., Götz, A. W., Kolossvari, I., Wong, K. F., Paesani, F., Vanicek, J., Wolf, R. M., Liu, J., Wu, X., Brozell, S. R., Steinbrecher, T., Gohlke, H., Cai, Q., Ye, X., Wang, J., Hsieh, M.-J., Cui, G., Roe, D. R., Mathews, D. H., Seetin, M. G., Salomon-Ferrer, R., Sagui, C., Babin, V., Luchko, T., Gusarov, S., Kovalenko, A., and Kollman, P. A. (2012) AMBER 12, University of California, San Francisco.

(53) Meagher, K. L., Redman, L. T., and Carlson, H. A. (2003) Development of polyphosphate parameters for use with the AMBER force field. *J. Comput. Chem.* 24, 1016–1025.

(54) Berendsen, H. J. C., Grigera, J. R., and Straatsma, T. P. (1987) The missing term in effective pair potentials. *J. Phys. Chem.* 91, 6269–6271.

(55) Götz, A. W., Williamson, M. J., Xu, D., Poole, D., Le Grand, S., and Walker, R. C. (2012) Routine microsecond molecular dynamics simulations with AMBER on GPUs. 1. Generalized Born. *J. Chem. Theory Comput.* 8, 1542–1555.

(56) Ryckaert, J. P., Ciccotti, G., Berendsen, H. J. C., and Hirasawa, K. (1977) Numerical integration of the cartesian equations of motion of a system with constraints: Molecular dynamics of n-alkanes. *J. Comput. Phys.* 23, 327–341.

(57) Miyamoto, S., and Kollman, P. A. (1992) Settle: An analytical version of the SHAKE and RATTLE algorithm for rigid water models. *J. Comput. Chem.* 13, 952–962.

(58) Egli, M., Pattanayek, R., and Pattanayek, S. (2007) Protein-protein interactions in the cyanobacterial KaiABC circadian clock. In *Models, Mysteries and Magic of Molecules* (Boeyens, J. C. A., and Ogilvie, J. F., Eds.) pp 283–299, Springer Publishers, Dordrecht, The Netherlands.

(59) Hayashi, F., Ito, H., Fujita, M., Iwase, R., Uzumaki, T., and Ishiura, M. (2004) Stoichiometric interactions between cyanobacterial clock proteins KaiA and KaiC. *Biochem. Biophys. Res. Commun.* 316, 195–202.

(60) van Zon, J. S., Lubensky, D. K., Altena, P. R. H., and ten Wolde, P. R. (2007) An allosteric model of circadian KaiC phosphorylation. *Proc. Natl. Acad. Sci. U.S.A.* 104, 7420–7425.

(61) Rust, M. J., Golden, S. S., and O’Shea, E. K. (2011) Light-driven changes in energy metabolism directly entrain the cyanobacterial circadian oscillator. *Science* 331, 220–223.

(62) Wood, T. L., Bridwell-Rabb, J., Kim, Y.-I., Gao, T., Chang, Y.-G., LiWang, A., Barondeau, D. P., and Golden, S. S. (2010) The KaiA protein of the cyanobacterial circadian oscillator is modulated by a redox-active cofactor. *Proc. Natl. Acad. Sci. U.S.A.* 107, 5804–5809.

(63) Pattanayek, R., Sidiqi, S. K., and Egli, M. (2012) Crystal structure of the redox-active cofactor DBMIB bound to circadian clock protein KaiA and structural basis for DBMIB’s ability to prevent stimulation of KaiC phosphorylation by KaiA. *Biochemistry* 51, 8050–8052.

(64) Kim, Y.-I., Vinyard, D. J., Ananyev, G., Dismukes, G. C., and Golden, S. S. (2012) Oxidized quinones signal onset of darkness directly to the cyanobacterial oscillator. *Proc. Natl. Acad. Sci. U.S.A.* 109, 17765–17769.

(65) Hochachka, P. W., and Somero, G. N. (1973) *Biochemical adaptation: Mechanism and process in physiological evolution*, Oxford University Press, Oxford, U.K.